**Supplemental Figure S1.** The dehydropipecolic acid isomer identified in plant extracts and the in vitro ALD1 DP product have identical GC retention times.

A, Overlay of extracted ion chromatograms (m/z 108) of plant-derived 2,3-DP and the metabolite that has been biochemically obtained in assays with recombinant ALD1 and L-Lys as the amino acid substrate. Samples have been extracted and derivatized to obtain the carboxylic acid methyl esters ("procedure A"), as described in the main article.

B, Co-injection of combined extracts yields a single peak with identical retention time and mass spectrum (compare Fig. 1C).
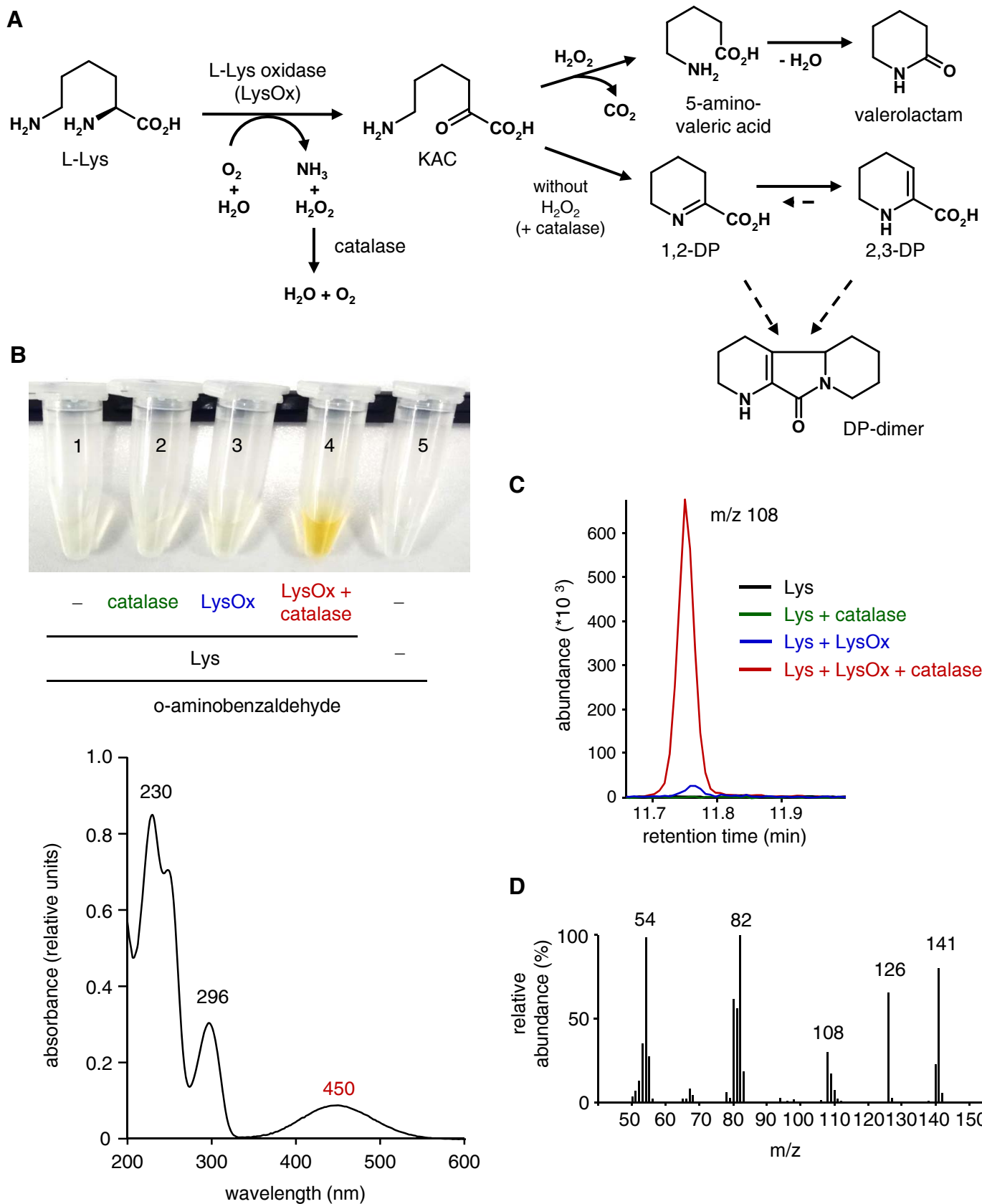
Supplemental Figure S2. Synthesis of 2,3-DP by L-Lysine oxidase (LysOx) from *Trichoderma viride*.

Supplemental Figure S2. continued.

A, Oxidative deamination of L-Lys by L-Lysine oxidase (LysOx) (modified from Pukin et al., 2010). The flavin-containing L-Lysine oxidase from *T. viride* catalyzes the oxidative deamination of L-Lys yielding ϵ-amino-α-ketocaproic acid (KAC) as formal product. This oxidation reaction requires one mole of O_2 and H_2O for each mole of L-Lys converted to KAC. As side-products of the oxidation process, NH_3 and H_2O_2 are formed in equimolar amounts. In the presence of catalase the generated H_2O_2 is eliminated, and the cyclic ketimine Δ^1-piperideine-2-carboxylate (Δ^1-P2C; alias 1,2-DP) is formed after spontaneous intramolecular cyclization of the open-chain form. 1,2-DP can tautomerize to the enamine Δ^2-P2C (alias 2,3-DP). The dehydropipecolic acid products can further dimerize and then undergo spontaneous dehydration and decarboxylation to form 1,2,3,4,5,6,7,8-octahydropyrido[3,2-α]-indolizin-10(4βH)-one (Hope et al., 1967), which is referred to as dehydropipecolic acid (DP)-dimer. This DP-dimer has also been observed in assays with recombinant ALD1, however to much lower extents and only at prolonged incubation times (> 12 h). In the absence of catalase, the inhibitory effects of H_2O_2 leads to an oxidative decarboxylation of 6-amino-2-ketocaproic acid and the formation of 5-aminovaleric acid as major LysOx-catalysed reaction product (Pukin et al., 2010). In our experimental setup, 5-aminovaleric acid was then further converted to valerolactam as reported by Bird et al. (2012).

B, Top: In order to characterize the product of the LysOx/catalase assay with L-Lys as substrate, the formation of the yellow dihydroquinazolinium complex of P2C with *o*-aminobenzaldehyde has been monitored as described in previous studies (Vogel and Davis, 1952; Misono et al., 1971; Kusakabe et al., 1980). Four different assay conditions can be seen from left to right, all of which contain L-Lys: control without enzyme (1), control using catalase only (2), an assay using LysOx without catalase (3) and a full assay using LysOx and catalase. Assays were incubated at 37° for at least 1 h before stopping the reaction and adding an equal amount of 10 mM *o*-aminobenzaldehyde to the reaction mixture. A yellow colour developed after incubation for more than 30 min at 37° C. Please note that the formation of an intense yellow adduct occurs solely in the reaction mixture containing LysOx and catalase and none of the other assays (1-3) or the control with *o*-aminobenzaldehyde alone (5).
Bottom: The UV-VIS spectrum of the yellow complex shows, besides absorption maxima in the UV region, a characteristic maximum at 450 nm (Soda et al., 1968; Kusakabe et al., 1980). Analyses were performed using an Agilent 1200 series HPLC system equipped with an Agilent 1200 Series G1315C Diode-array Detector SL (DAD SL) and a C18-RP (reverse phase) column (Zorbax Rapid resolution HAT SB-C18, 1.8 µm, 2.1x100 mm). The mobile phase was 0.1% formic acid in water (A) and in acetonitrile (B). The flow rate was 0.35 ml min^{-1} and the column temperature 25°C. 5 µl of an overnight assay were injected and eluted on a linear gradient. The spectrum of the HPLC-separated complex was recorded from 200 to 600 nm while the chromatogram was acquired at 230 nm.
Please note that the same yellowish complex has been obtained with the ALD1-derived 2,3-DP product (not shown). Since imines such as Δ^1-piperideine-derivatives can react as the heterocyclic enamine tautomers in the o-aminobenzaldehyde reaction (Harada et al., 1970; Hickmott, 1982), a discrimination of 1,2-DP and 2,3-DP is not possible with this assay.

C, Overlay of extracted ion chromatograms (m/z 108) after GC-MS analysis of the LysOx-derived reaction product with L-Lys as a substrate. Carboxylic acids in the samples were derivatized to their respective methyl esters by procedure A as described in the main text. As described in (B), four different assay setups were compared. The DP product was only detected in the full assays including LysOx, whereas the controls without substrate (L-Lys) or only containing catalase as enzyme did not yield any detectable reaction product. The reaction mixture containing both LysOx and catalase showed significantly more reaction product as the assay incubated only in the presence of LysOx.
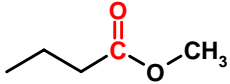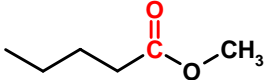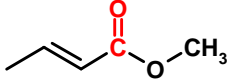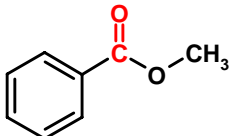
D, Mass spectrum of the reaction product obtained from L-Lys in the presence of LysOx and catalase, derivatized by procedure A. The reaction product was identified as 2,3-DP-methyl ester (Fig. 1C; compare main text).
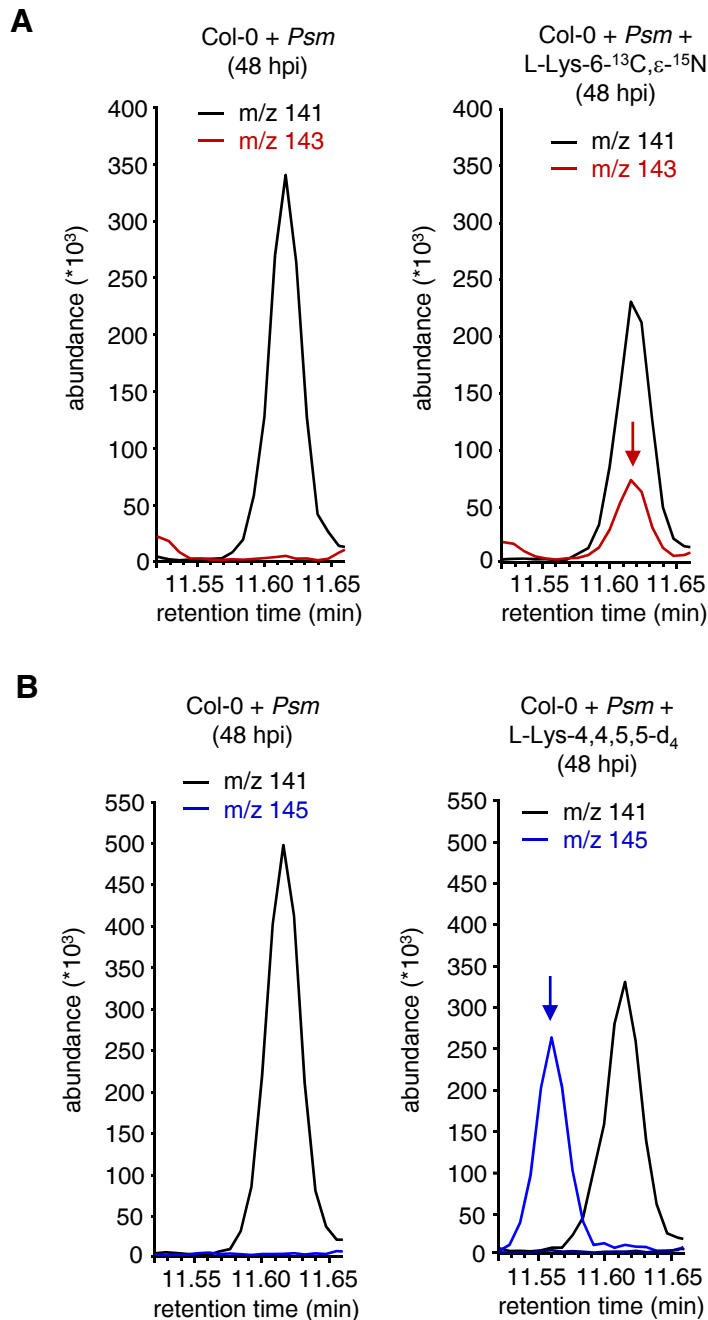
Supplemental Figure S3. In planta formation of isotope-labelled 2,3-dehydropipecolic acid versions. The products are identical to those detected in ALD1 in vitro assays .

A, Overlay of extracted ion chromatograms of m/z 141 (black - molecular ion of unlabelled <u>1a</u>; Fig. 1C) and m/z 143 (red - molecular ion of 6-^{13}C,^{15}N-labelled <u>1a</u>; Fig. 1D) of extract samples of *Psm*-inoculated Col-0 leaves. Left: *Psm*-infiltration only. Right: co-infiltration of *Psm* and L-Lys-6-^{13}C,ε-^{15}N. Leaf samples were harvested 48 h after treatment, extracted, and analyzed according to GC-MS procedure A. Please note the presence of 6-^{13}C,^{15}N-labelled 2,3-DP in the chromatogram of the L-Lys-6-^{13}C,ε-^{15}N-supplemented sample (arrow). Unlabeled 2,3-DP is formed from endogenous L-Lys in both cases.

B, Overlay of extracted ion chromatograms of m/z 141 (black - molecular ion of unlabelled <u>1a</u>; Fig. 1C) and m/z 143 (blue - molecular ion of 4,4,5,5-d$_4$-labelled <u>1a</u>; Fig. 1E) of extract samples of *Psm*-inoculated Col-0 leaves. Left: *Psm*-infiltration only. Right: co-infiltration of *Psm* and L-Lys-4,4,5,5-d$_4$. Leaf samples were harvested 48 h after treatment, extracted, and analyzed according to GC-MS procedure A. Please note the presence of d$_4$-labelled 2,3-DP in the chromatogram of the L-Lys-4,4,5,5-d$_4$-supplemented sample (arrow). Unlabeled 2,3-DP is formed from endogenous L-Lys in both cases.

compound	structure	C=O vibration (cm^{-1})
methyl butyrate		1761
methyl valerate		1760
methyl crotonate		1749
methyl benzoate		1747

Supplemental Figure S4. Wavenumbers of the infrared absorption bands of C=O stretching vibrations occurring in different carboxylic acid methyl esters, as determined by GC-FTIR analysis.

The carbonyl bond in the molecular structure of each compound is highlighted in red. Wavenumbers of C=O stretching vibrations are given in cm^{-1}.
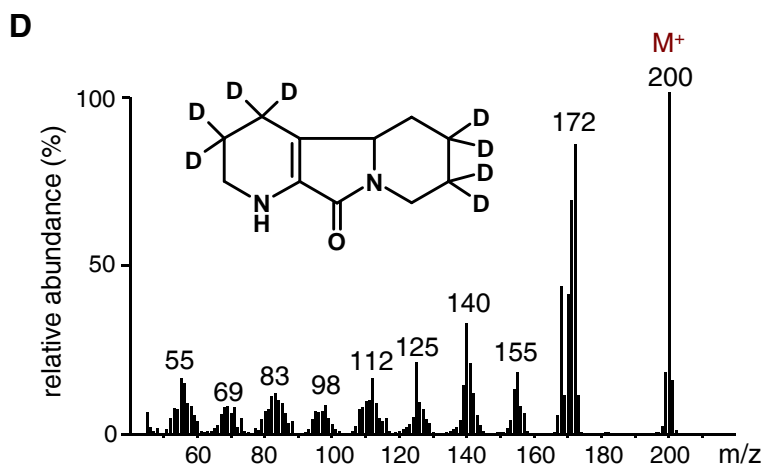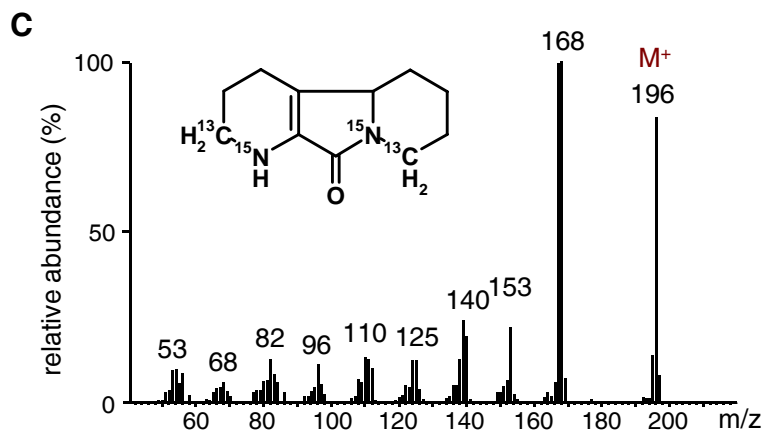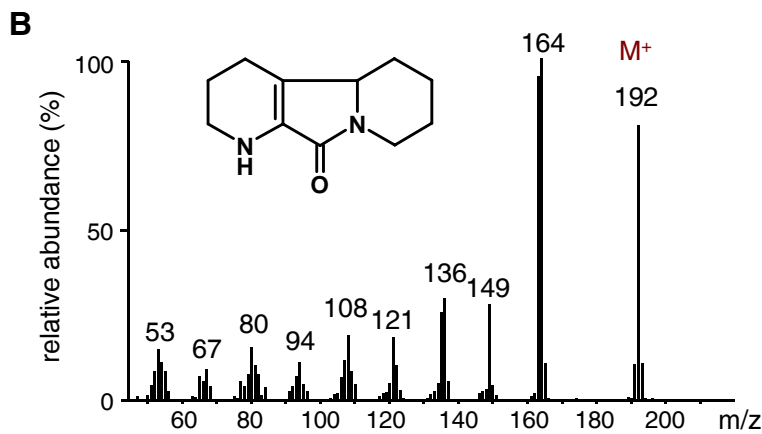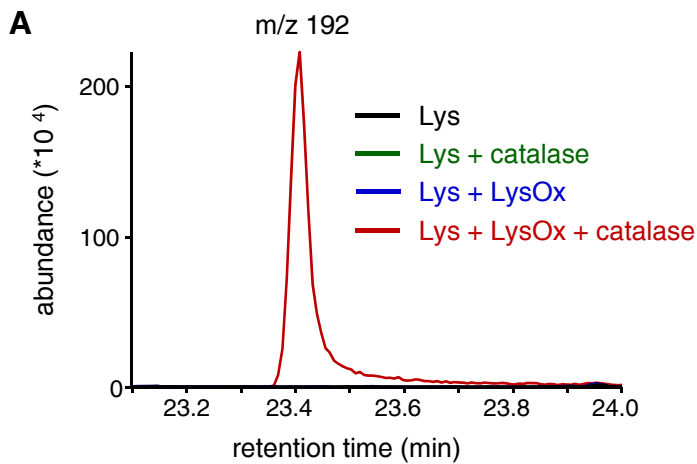
Supplemental Figure S5. In addition to 2,3-DP, the L-Lys-derived DP-dimer is detected in L-Lysine oxidase assays carried out in the presence of catalase.

The P2C may further dimerize and be transformed to 1,2,3,4,5,6,7,8-octahydropyrido[3,2-a]-indolizin-10(4b*H*)-one, the derivative of the DP-dimer (Hope et al., 1967). This DP-dimer has also been observed in assays with recombinant ALD1, however to much lower extents. The DP-dimer, which has been characterized in great detail by Horncastle and colleagues (1967) via GC-MS and ^{1}H-NMR, has been clearly identified exclusively in the assays yielding 2,3-DP as the main product.

A, Overlay of extracted ion chromatograms (m/z 192) after GC-MS analysis of the DP-dimer. Four different assay conditions were applied, all of which contain L-Lys: control without enzyme (black), control using catalase only (green), assay using LysOx without catalase (blue), and full assay using LysOx and catalase (red).

B, Mass spectrum and molecular structure of the DP-dimer derived from LysOx/catalase-mediated L-Lys conversion.

C, Mass spectrum and proposed structure of isotope-labelled DP-dimer after use of L-Lys-6-^{13}C,ε-^{15}N as the substrate in the combined LysOx/catalase assay.

D, Mass spectrum and proposed structure of isotope-labelled DP-dimer after use of L-Lys-4,4,5,5-d$_4$ as the substrate in the combined LysOx/catalase assay.
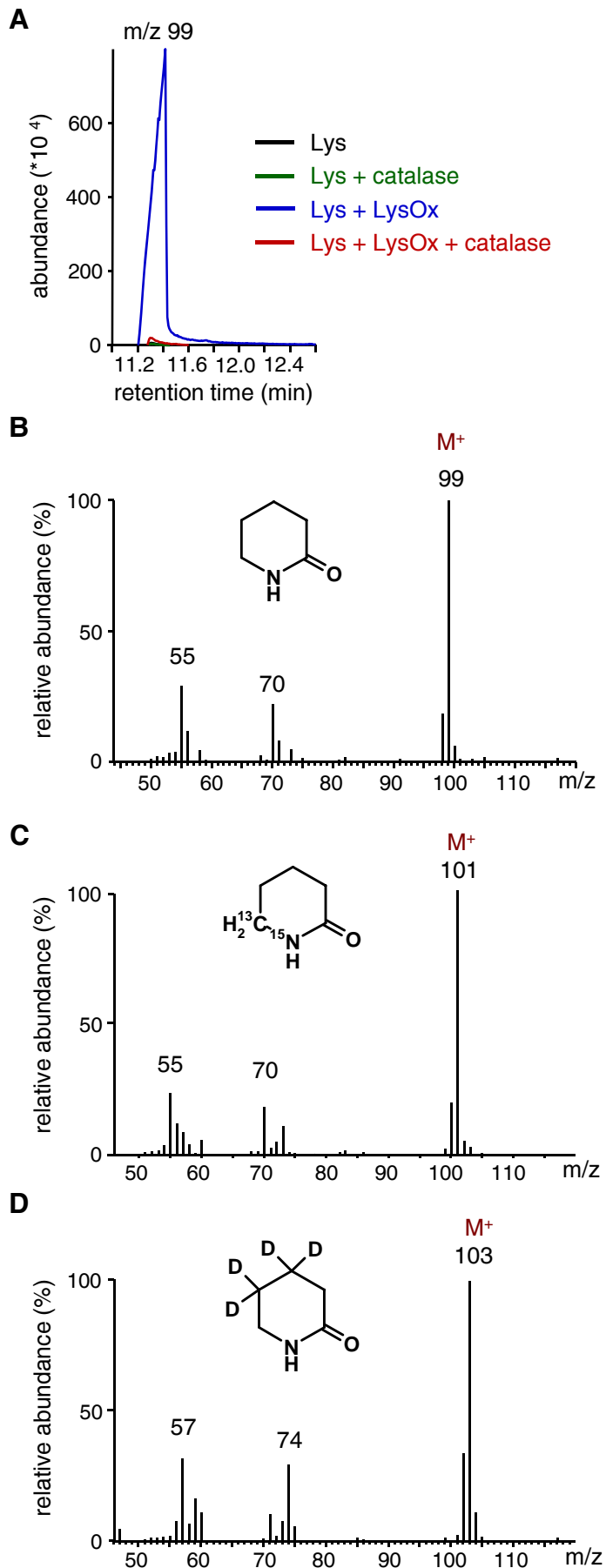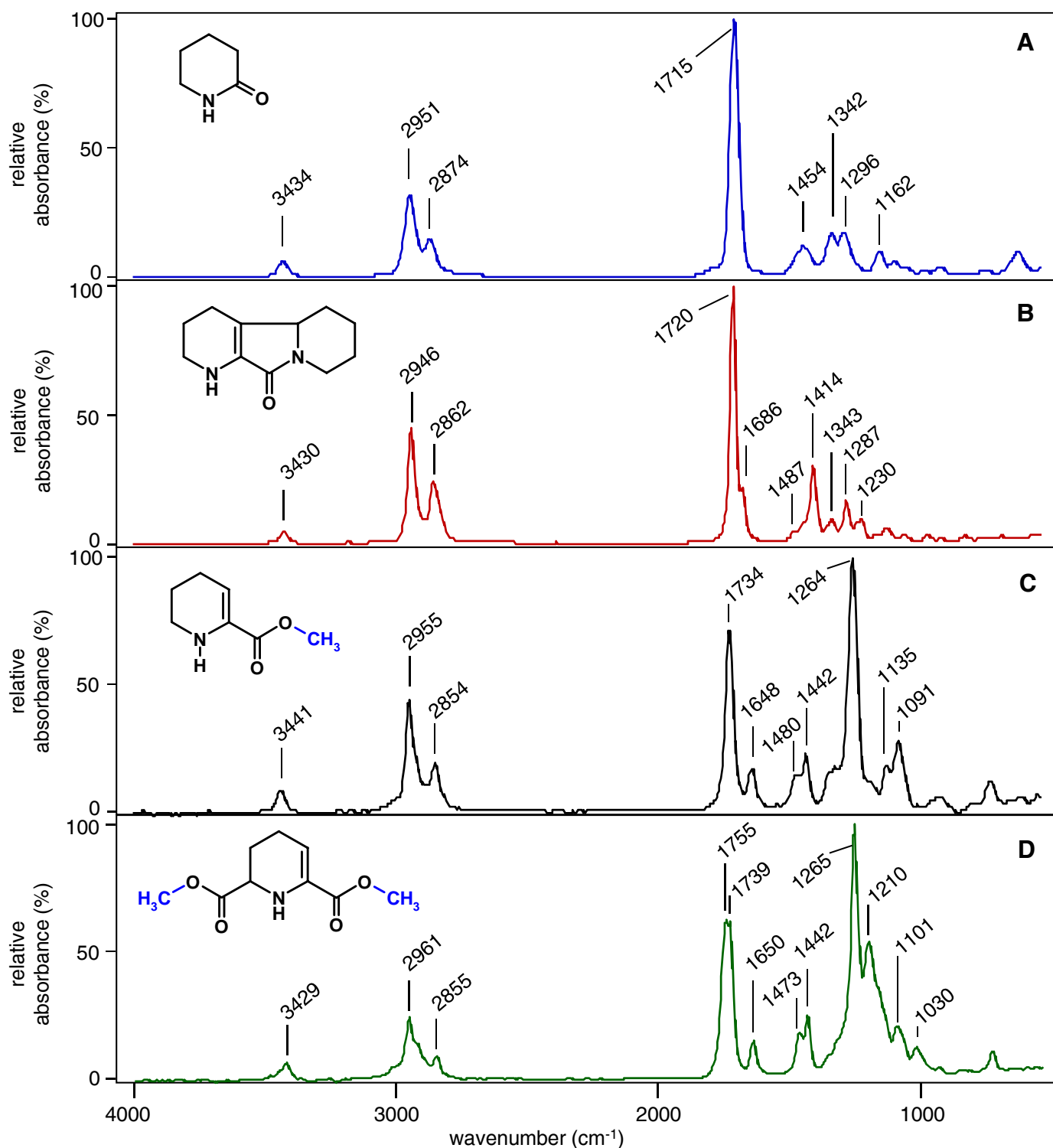
Supplemental Figure S6. Valerolactam is the main L-Lys-derived reaction product in L-Lysine oxidase assays performed in the absence of catalase.

A, Overlay of extracted ion chromatograms (m/z 99) after GC-MS analysis of valerolactam. Four different assay conditions were applied, all of which contain L-Lys: control without enzyme (black), control using catalase only (green), assay using LysOx without catalase (blue), and full assay using LysOx and catalase (red).

B, Mass spectrum and molecular structure of valerolactam derived from L-Lys conversion by LysOx only.

C, Mass spectrum and proposed structure of isotope-labelled valerolactam after use of L-Lys-6-^{13}C,ε-^{15}N as the substrate in the LysOx assay without catalase.

D, Mass spectrum and proposed structure of isotope-labelled DP-dimer after use of L-Lys-4,4,5,5-d$_4$ as the substrate in the LysOx assay without catalase.

Supplemental Figure S7. Infrared spectra of valerolactam, DP-dimer, 2,3-DP methyl ester, and 6-carboxy-2,3-DP dimethyl ester, as determined by GC-FTIR analyses.

Main IR absorption bands are indicated, and their assignment to functional groups is outlined in the main text. Please note the presence of an N-H stretching vibration in each of the spectra at ~3430-3440 cm^{-1}. The methyl groups introduced by derivatization (procedure A) are depicted in blue.

A, IR spectrum and molecular structure of valerolactam.

B, IR spectrum and molecular structure of DP-dimer.

C, IR spectrum and molecular structure of methlyated 2,3-dehydropipecolic acid (<u>1a</u>).

D, IR spectrum and molecular structure of dimethlyated 6-carboxy-2,3-dehydropipecolic acid (<u>2a</u>).
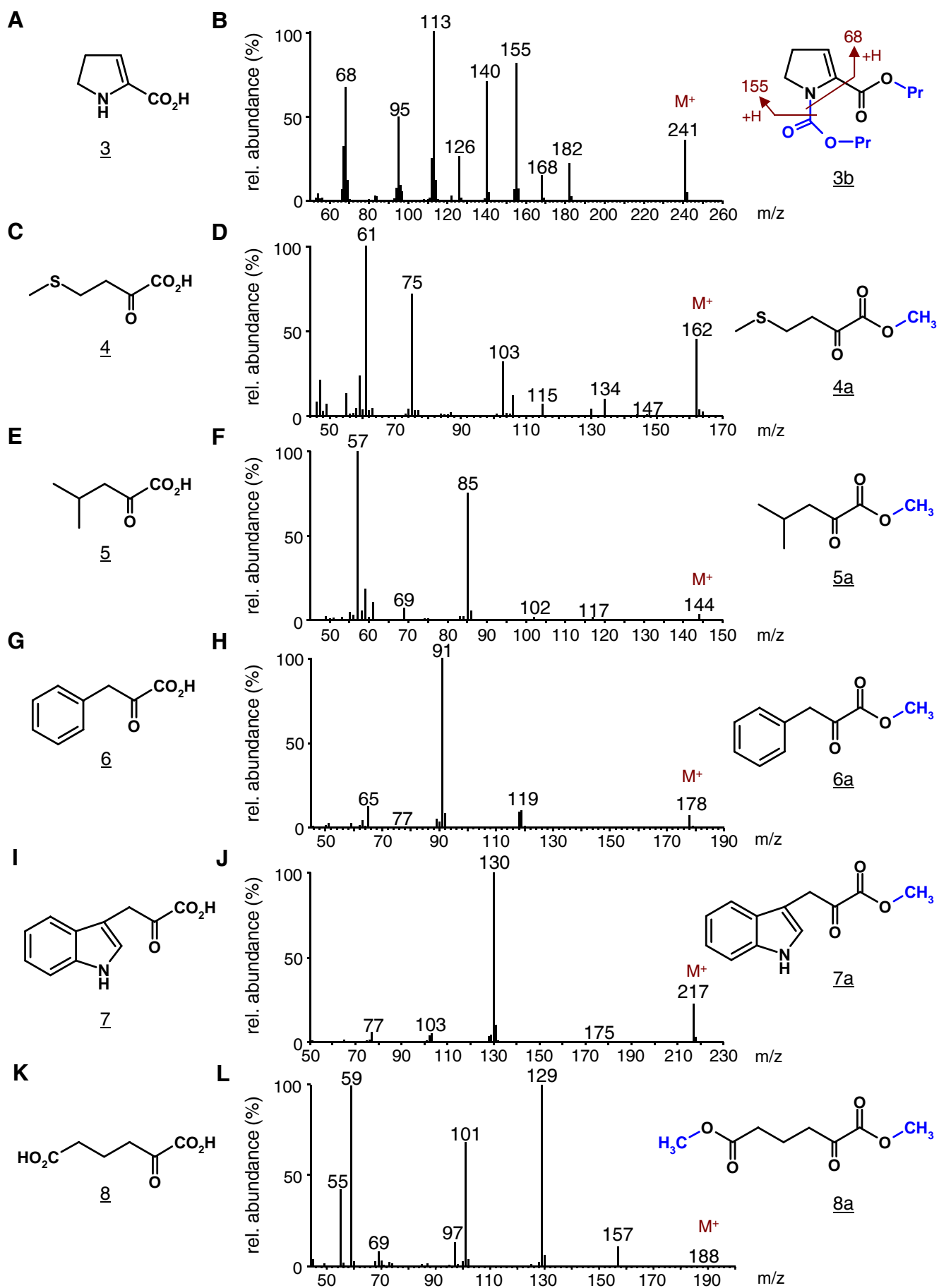
Supplemental Figure S8. Structures of non-derivatized and derivatized ALD1 transamination products and their mass spectra (as determined by GC-MS analysis).

Supplemental Figure S8. continued.

A, Structure of L-Orn-derived Δ^2-pyrroline-2-carboxylic acid (Δ^2-Pyr2C) (<u>3</u>). **B**, Mass spectrum and structure of propyl chloroformate-derivatized compound <u>3</u> (<u>3b</u>). The groups introduced by derivatization (GC-MS procedure B) are labelled in blue. Assignments of mass spectral fragments are indicated (M⁺ = molecular ion).

C, Structure of L-Met-derived α-ketomethionine (<u>4</u>). **D**, Mass spectrum and structure of the corresponding methyl ester (<u>4a</u>). The methyl group(blue) is introduced by derivatization (GC-MS procedure A).

E, Structure of L-Leu-derived α-ketoleucine (<u>5</u>). **F**, Mass spectrum and structure of the corresponding methyl ester (<u>5a</u>). The methyl group (blue) is introduced by derivatization (GC-MS procedure A).

G, Structure of L-Phe-derived phenylpyruvic acid (<u>6</u>). **H**, Mass spectrum and structure of the corresponding methyl ester (<u>6a</u>). The methyl group (blue) is introduced by derivatization (GC-MS procedure A).

I, Structure of L-Trp-derived indole-3-pyruvic acid (<u>7</u>). **J**, Mass spectrum and structure of the corresponding methyl ester (<u>7a</u>). The methyl group (blue) is introduced by derivatization (GC-MS procedure A).

K, Structure of L-amino adipic acid-derived α-ketoadipidc acid (<u>8</u>). **L**, Mass spectrum and structure of the corresponding dimethyl ester (<u>8a</u>). The methyl groups (blue) are introduced by derivatization (GC-MS procedure A).
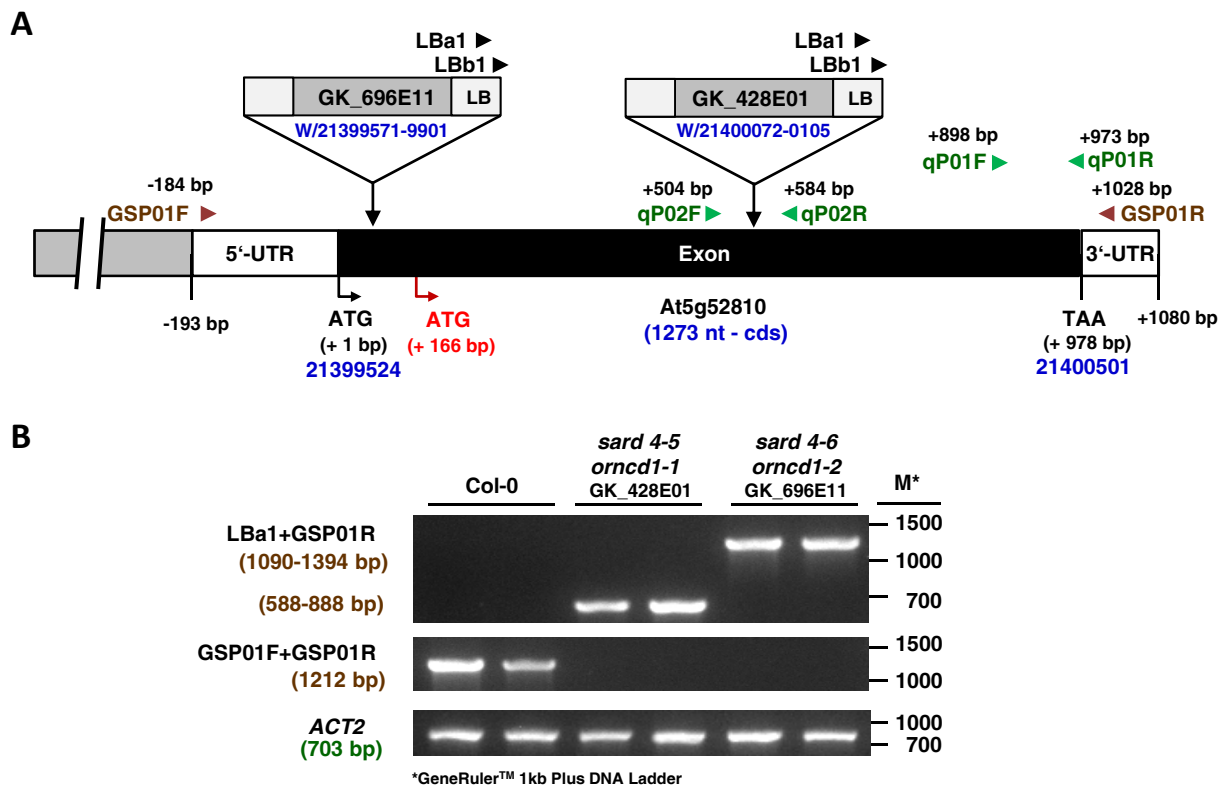
Supplemental Figure S9. Genomic organization of the *SARD4* (alias *ORNCD1*) mutant alleles *sard4-5* (*orncd1-1*; GK_428E01) and *sard4-6* (*orncd1-2*; GK_696E11) and characterization of *sard4* mutant lines.

A, At5g52810 gene model including *sard4-5* (*orncd1-1*; GK_428E01) and *sard4-6* (*orncd1-2*; GK_696E11) T-DNA insertion sites (boxes) and positions of respective primers (arrows) (Supplemental Table S2). The single exon of the *SARD4* gene is shown in black and the untranslated regions (UTR) in white. The positions of the T-DNA insertions in the two different lines are displayed as bars above the gene including the information on coordinates and orientation (w=upper strand), as published in the publicly available T-DNA insertion libraries (http://signal.salk.edu/cgi-bin/tdnaexpress). Black arrows above the boxes show the position and orientation of the left border primers (LBa1/LBb1) used for the characterization of the mutant lines. The gene-specific primers used for the characterization of the respective mutant lines were designed using the SALK primer design tool (http://signal.salk.edu/tdnaprimers.2.html) and are indicated in brown (GSP01F/R). Primers used for qPCR analysis are indicated in green. Please note that in addition to the start codon (ATG; position +1), the next possible ATG codon in frame with the coding sequence has been indicated in red (+166).

B, Characterization of *SARD4* mutant lines. The upper panel shows PCR analyses of genomic DNA from two representative WT plants (Col-0) and two plants for each of the respective T-DNA insertion lines using the T-DNA specific left border primers Lba1 and the gene–specific primer GSP01R. Expected PCR product sizes are indicated for each scenario on the left side. As expected, bands were only obtained in the mutant lines. In addition, PCRs with gene-specific primers located in the UTRs of *SARD4* only showed bands in the Col-0 wild-type plants and thus confirmed the presence of the T-DNA insertions in the mutant lines (middle panel). Amplified bands of *ACTIN2* (*ACT2*) are shown as controls (lower panel).

The predicted sites of T-DNA insertions are relatively central within the single exon of the gene for *sard4-5* and very close to the start of translation within the first 100 bp downstream of the start codon (ATG, +1) for *sard4-6* (A). This is consistent with the different sizes of bands resulting from PCR analyses with genomic DNA from *sard4-5* and *sard4-6* plants, respectively, and a combination of T-DNA left border (LBa1) and gene specific (GSP01R) primers annealing in the 3'-UTR region (B). The second ATG and possible start codon in frame with the coding sequence is located at position +166 of the nucleotide sequence, confirming the possibility that a shorter but functional version of *SARD4* is expressed in *sard4-6* (Fig. 8A, B).
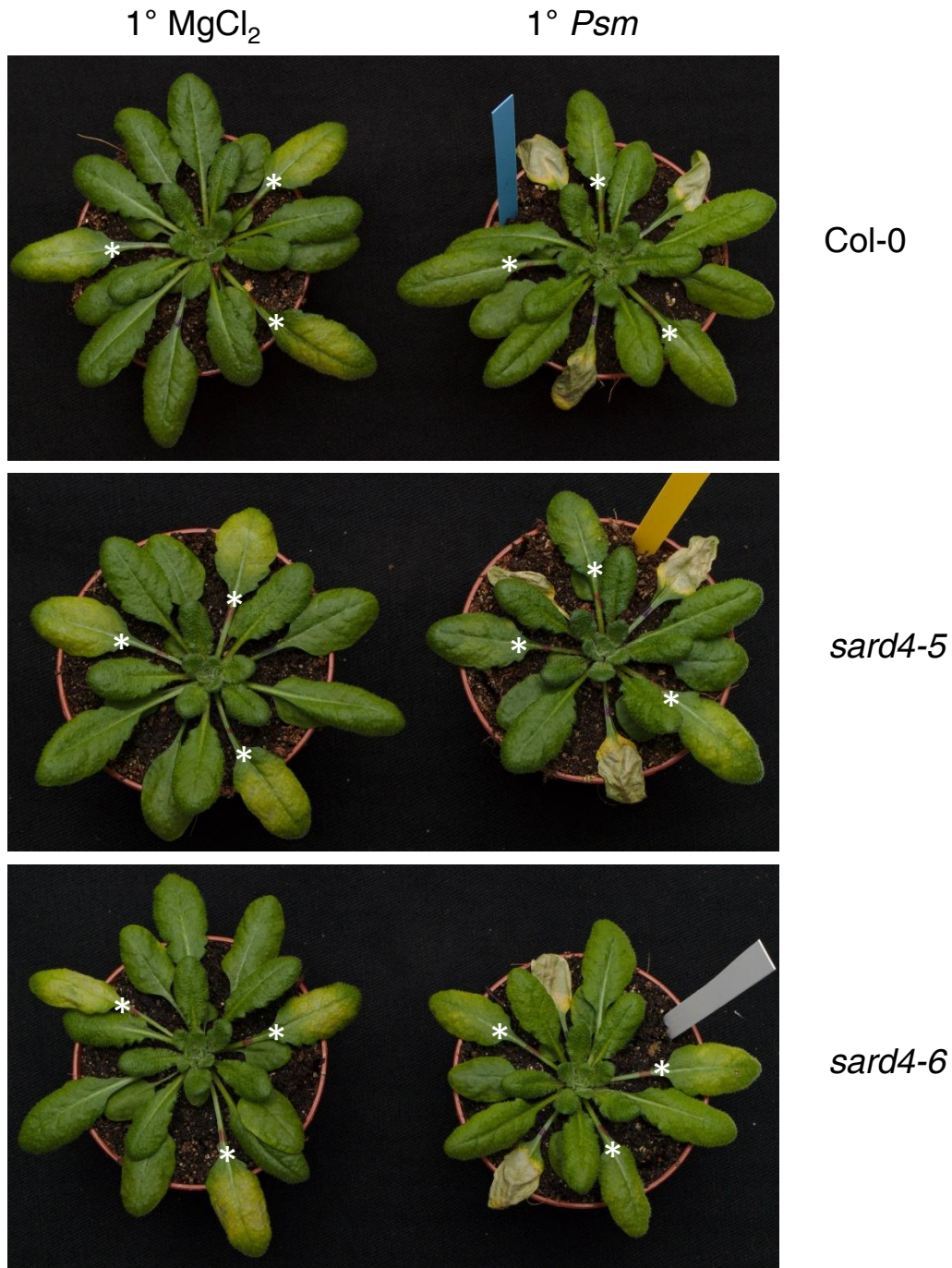
Supplemental Figure S10. Systemic acquired resistance (SAR) bioassay with the Col-0 wild-type, the *sard4-5* mutant, and the *sard4-6* mutant. Disease symptomology of representative plants.

Plants were infiltrated with 10 mM MgCl₂ (mock-treatment; left) or inoculated with a suspension of *P. syringae* pv. *maculicola* (*Psm*) (right) in three lower (1°) leaves. Two days later, both mock- and *Psm*-pre-treated plants were challenge-infected in three upper (2°) leaves with *Psm lux*. Representative plants were photographed 60 h after the 2°-challenge infection, just before a quantitative assessment of bacterial growth in 2° leaves by luminescence had been performed (Fig. 9B). The 2° leaves are marked with white asterisks at the bases of their leaf blades. Please note the distinct chlorotic disease symptoms in the 2° leaves of mock-pretreated plants. They appear more pronounced in the 2° leaves of *sard4* mutants compared to the wild-type. The disease symptoms are severely reduced in the *Psm*-pre-treated plants of all the lines under investigation, indicating SAR establishment in all the lines. However, the 2° leaves of the SAR-induced *sard4-5* line (right) appear slightly more chlorotic than those of the SAR-induced wild-type. The amount of leaf yellowing is usually correlated with the bacterial proliferation in the *P. syringae*-infected leaves (Fig. 9B).
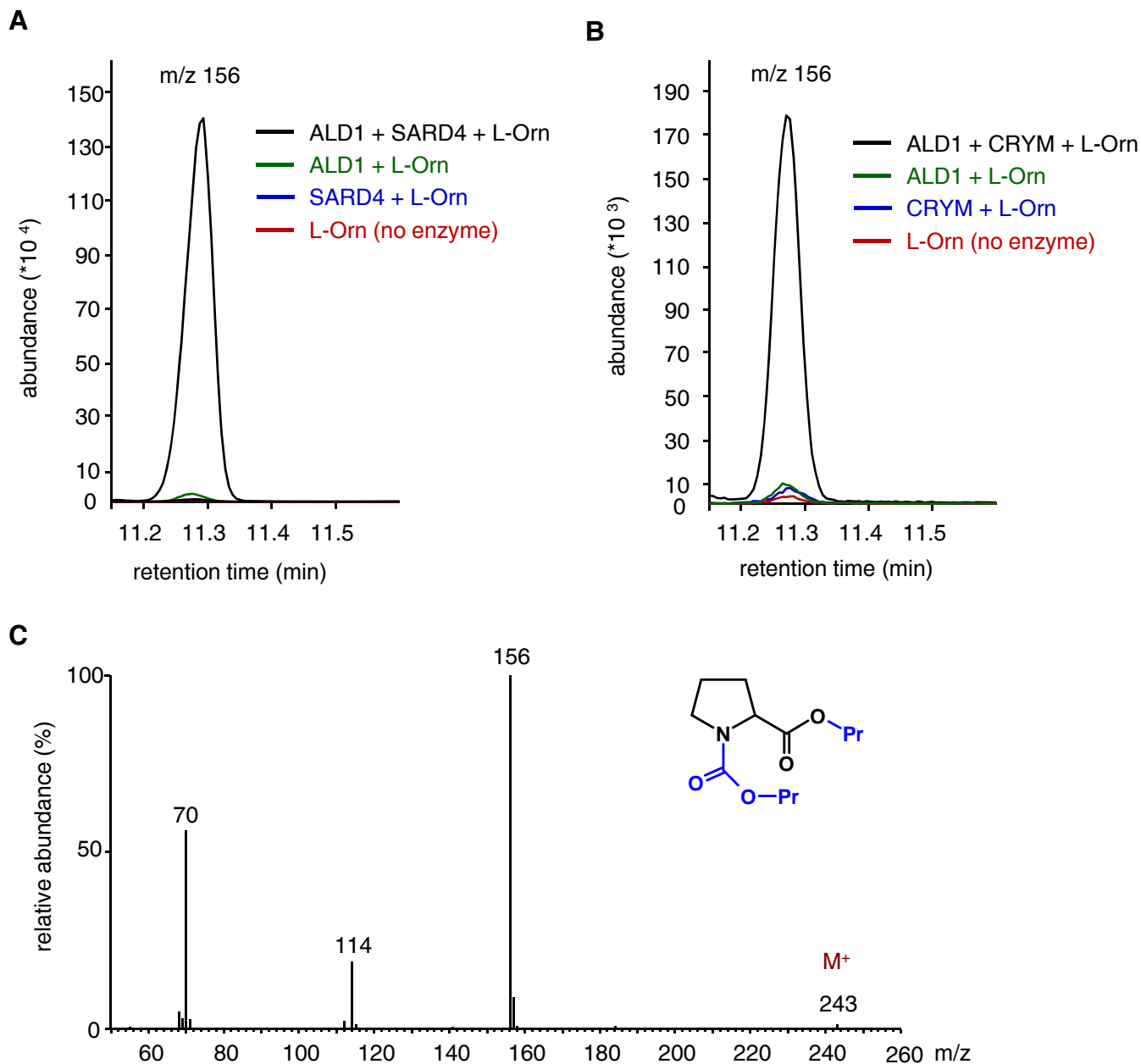
Supplemental Figure S11. Coupled in vitro assays with Arabidopsis ALD1 and SARD4, or with ALD1 and the human reductase CRYM yield proline with L-Orn as substrate.

A, In vitro enzyme activity assays containing purified recombinant enzymes and 20 mM L-Orn, 20 mM pyruvate, 5 mM $MgCl_2$, 100 μM pyridoxal- 5′- phosphate (PLP) and 200 μM NADH in 20 mM Tris buffer, pH 8.0. Incubation time 16 h (see Fig. 7 for further details). Black: coupled assay with ALD1 and SARD4; green: assay with ALD1 only, blue: assay with SARD4 only; red: assay mix without enzyme. Segments of overlaid ion chromatograms (m/z 156) are depicted after applying "workup procedure B". The peak at 11.3 min corresponds to propyl chloroformate-derivatized Pro.

B, Overlaid ion chromatograms from in vitro activity assays analogous to (A), with ALD1 and CRYM (black), with ALD1 only (green), with CRYM only (blue), and without enzyme (red).

C, Mass spectrum and chemical structure of chloroformate-derivatized Pro derived from coupled ALD1/SARD4 assays (identical to the mass spectrum of commercial L-Pro; see Návarová et al., 2012). The propyl- and propyl carbamate-groups introduced by derivatization are depicted in blue. The molecular ion (M+) is indicated.